



1980 North Atlantic Avenue • Suite 230 • Cocoa Beach, FL 32931 • 321-783-9735 • [www.ensco.com](http://www.ensco.com)

## **Applied Meteorology Unit (AMU)**

### **Quarterly Report**

### **Second Quarter FY-04**

**Contract NAS10-01052**

**30 April 2004**

## Distribution

NASA HQ/M/F. Gregory  
NASA KSC/AA/J. Kennedy  
NASA KSC/MK/M. Wetmore  
NASA KSC/PH/ M. Wetmore  
NASA KSC/PH-A2/D. Lyons  
NASA KSC/PH/M. Leinbach  
NASA KSC/PH/S. Minute  
NASA KSC/PH-A/J. Guidi  
NASA KSC/YA/J. Heald  
NASA KSC/YA-C/D. Bartine  
NASA KSC/YA-D/H. Delgado  
NASA KSC/YA-D/J. Madura  
NASA KSC/YA-D/F. Merceret  
NASA JSC/MA/W. Parsons  
NASA JSC/MS2/C. Boykin  
NASA JSC/ZS8/F. Brody  
NASA JSC/ZS8/R. Lafosse  
NASA MSFC/ED41/W. Vaughan  
NASA MSFC/ED44/D. Johnson  
NASA MSFC/ED44/B. Roberts  
NASA MSFC/ED44/S. Deaton  
NASA MSFC/MP71/S. Glover  
NASA DFRC/RA/J. Ehernberger  
45 WS/CC/R. LaFebre  
45 WS/DO/P. Broll  
45 WS/DOR/T. McNamara  
45 WS/DOR/J. Moffitt  
45 WS/DOR/J. Tumbiolo  
45 WS/DOR/K. Winters  
45 WS/DOR/J. Weems  
45 WS/SY/D. Hajek  
45 WS/SYA/B. Boyd  
45 WS/SYO/F. Flinn  
45 WS/SYR/W. Roeder  
45 MXG/CC/B. Presley  
45 MXG/LGP/R. Fore  
45 SW/SESL/D. Berlinrut  
45 OG/CC/G. Billman  
CSR 4140/H. Herring  
CSR 7000/M. Maier  
SMC/RNP/D. Salm  
SMC/RNP/T. Knox  
SMC/RNP/R. Bailey  
SMC/RNP (PRC)/P. Conant  
HQ AFSPC/XOSW/A. Gibbs  
HQ AFWA/CC/C. Benson  
HQ AFWA/DNX/W. Cade  
HQ AFWA/DN/M. Zettlemoyer  
HQ USAF/XOW/R. Clayton  
HQ USAF/XOWX/J. Lanicci  
NOAA "W/NP"/L. Uccellini  
NOAA/OAR/SSMC-I/J. Golden  
NOAA/NWS/OST12/SSMC2/J. McQueen  
NOAA Office of Military Affairs/N. Wyse  
NWS Melbourne/B. Hagemeyer  
NWS Southern Region HQ/"W/SRH"/X. W. Proenza  
NWS Southern Region HQ/"W/SR3"/D. Smith  
NWS/"W/OST1"/B. Saffle  
NSSL/D. Forsyth  
NSSL/C. Crisp  
30 WS/SY/M. Schmeiser  
30 WS/SYR/L. Wells  
30 WS/CC/C. Keith  
30 WS/DO/S. Saul  
30 SW/XPE/R. Ruecker  
88 WS/WES/K. Lehneis  
88 WS/WES/G. Marx  
46 WS//DO/M. Treu  
46 WS/WST/A. Michels  
412 OSS/OSWM/P. Harvey  
FSU Department of Meteorology/P. Ray  
FSU Department of Meteorology/H. Fuelberg  
NCAR/J. Wilson  
NCAR/Y. H. Kuo  
NOAA/ERL/FSL/J. McGinley  
Office of the Federal Coordinator for Meteorological  
Services and Supporting Research/J. Harrison, R. Dumont  
Boeing Houston/S. Gonzalez  
Aerospace Corp/T. Adang  
ACTA, Inc./B. Parks  
ENSCO, Inc./T. Wilfong  
ENSCO, Inc./E. Lambert  
ENSCO, Inc./A. Dianic

## EXECUTIVE SUMMARY

This report summarizes the Applied Meteorology Unit (AMU) activities for the Second Quarter of Fiscal Year 2004 (January – March 2004). A detailed project schedule is included in the Appendix.

### Task Objective Lightning Probability Forecast: Phase I

- Goal* Develop a set of statistical equations to forecast the probability of lightning occurrence for the day. This will aid forecasters in evaluating flight rules and determining the probability of launch commit criteria violations, as well as preparing forecasts for ground operations.
- Milestones* Two memorandums were distributed that describe issues in the Man-computer Interactive Data Access System (McIDAS) and HUGE program sounding analysis algorithms.
- Discussion* Due to some unrealistic stability parameter values calculated by McIDAS, the HUGE program algorithms were examined for their utility in this task. The HUGE code has several significant logic errors and cannot be used.

### Task Mesonet Temperature and Wind Climatology

- Goal* Identify biases in the wind and temperature observations at individual or groups of sensors based on location, weather conditions, and sensor exposure. Any deviations in the data field could adversely affect forecasts and analyses for ground, launch, and landing operations.
- Milestones* The nine-year climatology of hourly mean temperatures and standard deviations at all towers by month was completed. A graphical user interface (GUI) was created to display these values on the Internet.
- Discussion* The climatology values are displayed using Microsoft® Excel® pivot charts and tables, and geographical contour plots of the tower network. A GUI was developed for the Internet that allows easy navigation throughout the data sets.

### Task Severe Weather Forecast Decision Aid

- Goal* Create a new forecast aid to improve the severe weather watches and warnings meant for the protection of Kennedy Space Center (KSC) / Cape Canaveral Air Force Station (CCAFS) personnel and property.
- Milestones* Stability indices calculated from the morning sounding at CCAFS for February, March and April 1989 – 2003 were added to the AMU database of severe weather events. About 30% of the local severe weather events occur during these three months.
- Discussion* Local severe weather events documented by the National Weather Service office at Melbourne (NWS MLB) were missing in the database of storm events at the National Climatic Data Center (NCDC). The AMU database of severe weather events, based on the NCDC archive, will be updated with the assistance from NWS MLB personnel.

### Task Shuttle Ascent Camera Cloud Obstruction Forecast

- Goal* In response to a request from the Shuttle Program to implement a recommendation of the Columbia Accident Investigation Board, develop a model to forecast the probability that at least three of the shuttle ascent imaging cameras will have a view of the shuttle launch vehicle (LV) unobstructed by cloud at any time from launch to Solid Rocket Booster (SRB) separation.
- Milestones* A 3-D computer model was developed to generate line-of-sight information from ground and airborne cameras to the LV along its ascent path to SRB separation. The model was randomly seeded with cloud fields and viewing probabilities were computed for selected cloud scenarios.
- Discussion* An analysis of the sensitivity of viewing probabilities to upgrades of the camera network was developed in collaboration with the Shuttle Launch Director, the Intercenter Photo Working Group at KSC, and the 45th Weather Squadron Shuttle Launch Weather Officer.

Task      Anvil Transparency Relationship to Radar Reflectivity

*Goal*      Determine if products from the NWS MLB WSR-88D radar can be used to analyze anvil cloud transparency, an important element in forecasting launch commit criteria. Opaque anvils can carry an electrical charge. If a vehicle flies through such a charge, it could trigger lightning and be destroyed.

*Milestones*      Forty-five (45) days during the summer of 2003 were identified with thunderstorm anvil cirrus clouds over Weather Station B (KTTS), based on a comparative analysis of satellite imagery and the KTTS observations.

*Discussion*      The WSR-88D Layer Reflectivity Maximum products for the 45 case days are being processed by the NOAA Radar Operations Center. These will be used in a comparative analysis with the surface observations of anvil transparency from KTTS.

## Table of Contents

EXECUTIVE SUMMARY .....	iii
AMU ACCOMPLISHMENTS DURING THE PAST QUARTER.....	1
SHORT-TERM FORECAST IMPROVEMENT .....	1
Objective Lightning Probability: Phase I (Ms. Lambert and Mr. Wheeler).....	1
Mesonet Temperature and Wind Climatology (Mr. Case and Dr. Bauman).....	3
Severe Weather Forecast Decision Aid (Mr. Wheeler and Dr. Short).....	8
Shuttle Ascent Camera Cloud Obstruction Forecast (Dr. Short and Mr. Lane).....	10
INSTRUMENTATION AND MEASUREMENT .....	14
I&M and RSA Support (Mr. Wheeler and Dr. Bauman) .....	14
Anvil Transparency Relationship to Radar Reflectivity (Dr. Short and Mr. Wheeler).....	15
AMU CHIEF’S TECHNICAL ACTIVITIES (DR. MERCERET).....	18
AMU OPERATIONS.....	18
REFERENCES.....	20
List of Acronyms.....	21
Appendix A .....	23

## **SPECIAL NOTICE TO READERS**

Applied Meteorology Unit (AMU) Quarterly Reports are now available on the Wide World Web (WWW) at <http://science.ksc.nasa.gov/amu/>.

The AMU Quarterly Reports are also available in electronic format via email. If you would like to be added to the email distribution list, please contact Ms. Winifred Lambert (321-853-8130, [lambert.winifred@ensco.com](mailto:lambert.winifred@ensco.com)). If your mailing information changes or if you would like to be removed from the distribution list, please notify Ms. Lambert or Dr. Francis Merceret (321-867-0818, [Francis.J.Merceret@nasa.gov](mailto:Francis.J.Merceret@nasa.gov)).

## **BACKGROUND**

The AMU has been in operation since September 1991. Tasking is determined annually with reviews at least semi-annually. The progress being made in each task is discussed in this report with the primary AMU point of contact reflected on each task and/or subtask.

## **AMU ACCOMPLISHMENTS DURING THE PAST QUARTER**

### ***SHORT-TERM FORECAST IMPROVEMENT***

#### **OBJECTIVE LIGHTNING PROBABILITY: PHASE I (MS. LAMBERT AND MR. WHEELER)**

The 45th Weather Squadron (45 WS) forecasters include a probability of thunderstorm occurrence in their daily morning briefings. This information is used by personnel involved in determining the possibility of violating Launch Commit Criteria (LCC), evaluating Flight Rules (FR), and daily planning for ground operation activities on Kennedy Space Center/Cape Canaveral Air Force Station (KSC/CCAFS). Much of the current lightning probability forecast is based on a subjective analysis of model and observational data. The forecasters requested that a lightning probability forecast tool based on statistical analysis of historical warm-season data be developed. Such a tool would increase the objectivity of the daily thunderstorm probability forecast. The AMU is developing statistical lightning forecast equations that will provide a lightning occurrence probability for the day by 1100 UTC (0700 EDT) during the months May – September (warm season). The tool will be based on the results from several research projects. If tests of the equations show that they improve the daily lightning forecast, the AMU will develop a PC-based tool from which the daily probabilities can be displayed by the forecasters.

The three data types to be used in this task were described in previous AMU Quarterly Reports (Q4 FY03 and Q1 FY04):

- Cloud-to-Ground Lightning Surveillance System data,
- 1200 UTC sounding data from synoptic sites in Florida, and
- 1000 UTC CCAFS sounding (XMR) data.

Ms. Lambert is using the S-PLUS<sup>®</sup> software package (Insightful Corporation 2000) to process and analyze the data, and to develop the lightning forecast equations.

Ms. Lambert is using the XMR sounding data to calculate the stability parameters normally available to the forecasters through the Meteorological Interactive Data Display System (MIDDS). MIDDS uses the Man-computer Interactive Data Access System (McIDAS) software (Lazzara et al. 1999) for processing and displaying the sounding data. The McIDAS algorithms that process the sounding data will be used in this task to ensure that the calculated stability parameter values will be consistent with those available to the forecasters. The list of parameters to be calculated was in the previous AMU Quarterly Report (Q1 FY04).

### LFC Algorithm Issues

Certain issues arose when Ms. Lambert calculated the level of free convection (LFC) with the McIDAS algorithms. This value is necessary along with the equilibrium level (EL) to calculate convective available potential energy (CAPE) and convective inhibition (CIN). She noticed in certain soundings that the LFC was calculated to be below the lifting condensation level (LCL), a physical impossibility. There are three methods of parcel selection in McIDAS for calculating the LFC, EL, CAPE, and CIN: 1) mixed boundary layer parcel, 2) level in sounding with highest equivalent potential temperature ( $\theta_e$ ), and 3) surface parcel at the forecast maximum temperature and dew point temperature. The issue of the LFC being lower than the LCL occurred with all three methods, but was especially prevalent when using a surface parcel at the forecast maximum temperature. LFC values ranged from within just a few millibars of the LCL to 6300 mb. There were also some negative LFC values down to -2500 mb. If the McIDAS algorithm is able to calculate an LFC and an EL, CAPE and CIN will be calculated. If the LFC value is unrealistic, the resulting CAPE value will be incorrect and misleading to forecasters. The issue is caused by the equations and assumptions used in the code rather than bad data quality.

The LCL and LFC are calculated using two different methods. The LCL algorithm assumes that the dew point temperature at the surface is equal to that at the LCL as a first guess. It then does a rather complicated iteration until it finds a pressure where the parcel potential temperature ( $\theta$ ) and dew point temperature are close to those of the environment. This is considered to be the pressure of the LCL ( $P_{LCL}$ ). The LFC pressure ( $P_{LFC}$ ) is computed where the parcel wet adiabat crosses the observed temperature profile. The elements in the LFC algorithm equations are in Figure 1.

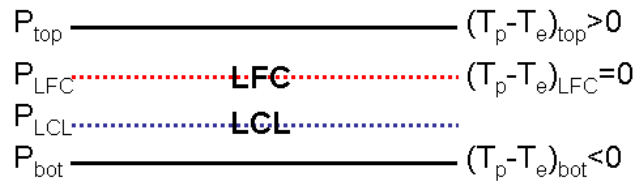


Figure 1. Schematic of physical configuration of the values used in McIDAS to calculate the LFC pressure. The solid black lines represent observed levels in the sounding, the dotted blue line represents the LCL, and the dotted red line represents the LFC. The  $P$  values on the left represent the pressure at each of the levels ( $P_{top} < P_{LFC} < P_{LCL} < P_{bot}$ ), and  $T_p - T_e$  values on the right represent the temperature difference between the parcel and environment at each of the levels.  $T_p - T_e$  is not calculated for the LCL in McIDAS.

The pressure at the LFC is calculated using the following procedures:

- Calculate the temperature of the lifted parcel ( $T_p$ ) at all observed levels in the sounding.
- Subtract the temperature of the environment ( $T_e$ ) from  $T_p$  and at each level.
- Locate the first observed level above the surface where  $T_p - T_e > 0$  **and**  $P_{LFC} < P_{LCL}$  (i.e. LFC physically higher than LCL). This is assumed to be the first observed level above the actual level of the LFC and has the pressure  $P_{top}$  and difference  $(T_p - T_e)_{top}$  in Figure 1.
- Identify the first observed level below the LFC with the pressure  $P_{bot}$  and difference  $(T_p - T_e)_{bot}$  in Figure 1.
- Calculate pressure of the LFC ( $P_{LFC}$ ) with the equation

$$P_{LFC} = P_{bot} + [P_{top} - P_{bot}] \left[ \frac{0 - (T_p - T_e)_{bot}}{(T_p - T_e)_{top} - (T_p - T_e)_{bot}} \right].$$

- The 0 in the numerator on the right-hand-side represents  $(T_p - T_e)_{LFC}$ , assuming  $T_p = T_e$  at the LFC.
- The algorithm also assumes that  $(T_p - T_e)_{bot} < 0$ .

A thorough analysis of the  $(T_p - T_e)_{bot}$  values for several soundings reveals that it is not always  $< 0$  when the LCL and LFC are between the same two observed levels, as in Figure 1. In these cases the ratio in the second term on the right-hand-side of the equation is the source for the erroneous  $P_{LFC}$  values. The magnitude and sign of  $P_{LFC}$  depend on the magnitudes of  $(T_p - T_e)_{top}$  and  $(T_p - T_e)_{bot}$  when they are both positive. Note that in the second term on the right-hand-side of the equation,  $[P_{top} - P_{bot}]$  is always negative, and when  $(T_p - T_e)_{bot} > 0$ , the numerator  $0 - (T_p - T_e)_{bot}$  in the ratio is always negative. The product of these two values will then be positive. Erroneous  $P_{LFC}$  values occur under the following conditions:

- When  $(T_p - T_e)_{top}$  and  $(T_p - T_e)_{bot}$  are both positive, the denominator,  $[(T_p - T_e)_{top} - (T_p - T_e)_{bot}]$ , becomes small, making the resulting magnitude of  $P_{LFC}$  erroneously large, but possibly within a realistic range of values.
- When  $(T_p - T_e)_{top}$  and  $(T_p - T_e)_{bot}$  are close in value, their difference is very small and an unrealistically large magnitude of  $P_{LFC}$  will result.
- The sign of  $P_{LFC}$  depends on which value is greater:
  - If  $(T_p - T_e)_{top} > (T_p - T_e)_{bot}$ , then  $[(T_p - T_e)_{top} - (T_p - T_e)_{bot}] > 0$  and  $P_{LFC} > 0$ .
  - If  $(T_p - T_e)_{top} < (T_p - T_e)_{bot}$ , then  $[(T_p - T_e)_{top} - (T_p - T_e)_{bot}] < 0$  and  $P_{LFC}$  will have a very small magnitude or be less than 0.

#### ***Actions Taken on LFC Issues***

Ms. Lambert did not investigate why the difference in the LCL and LFC algorithms would sometimes result in erroneous LFC values, but did bring it to the attention of the McIDAS Help Desk. They will enact an interim solution to set the LFC temperature and pressure equal to those of the LCL when the LFC pressure is greater than and within 2.5 mb of the LCL. Ms. Lambert sent other soundings to show that the difference can be greater than 2.5 mb, and suggested that a better solution may be to set the LFC values equal to the LCL values when they are between the same observed levels in the sounding and  $(T_p - T_e)_{top}$  and  $(T_p - T_e)_{bot}$  are both positive. However, they are scheduling a new release of the McIDAS code to customers and will not have time to look at the soundings or consider her suggestion until after the release in May. Ms. Lambert wrote a memorandum titled “Changes to Sounding Analysis Algorithm in McIDAS” that outlines this and other issues found in the code.

Ms. Lambert informed Mr. Johnny Weems about the LFC issues with McIDAS, and he suggested looking at the algorithms in another program available on MIDDs called HUGE. The HUGE program was acquired several years ago from the National Severe Storms Laboratory. It analyzes sounding data and calculates many of the same stability parameters as the McIDAS program. Mr. Rick Kulow of Computer Sciences Raytheon (CSR) provided the code and a sample input file to test the program. While testing and analyzing the algorithms and their output, Ms. Lambert noticed several spelling and logic errors in the algorithms. She summarized her findings in the memorandum titled “Errors in the HUGE Program”, and decided that the algorithms in this program would not be helpful in this task given the uncertainty of their accuracy. Ms. Lambert will meet with Mr. Bill Roeder and Mr. Johnny Weems to determine which parameters output from McIDAS should be used as predictors in the lightning forecast equations.

For more information on this work and for copies of the memoranda mentioned, contact Ms. Lambert at 321-853-8130 or [lambert.winifred@ensco.com](mailto:lambert.winifred@ensco.com).

#### **MESONET TEMPERATURE AND WIND CLIMATOLOGY (MR. CASE AND DR. BAUMAN)**

Forecasters at the 45 WS use the wind and temperature data from the KSC/CCAFS tower network to evaluate LCC and to issue and verify temperature and wind advisories, watches, and warnings for ground operations. The Spaceflight Meteorology Group (SMG) also uses these data when evaluating FR for Shuttle landings at the KSC Shuttle Landing Facility (SLF). Unidentified sensor and/or exposure biases in these measurements at any of the towers could adversely affect an analysis, forecast, or verification for all of these operations. In addition, substantial

variations in temperature and wind speed can occur due to geographic location or prevailing wind direction. Forecasters need to know if any towers exhibit a consistent bias in temperature and/or wind speed, and the typical geographical and diurnal variations of temperature and wind speed throughout the tower network. The AMU was tasked to identify any systematic biases, geographical variability, or meteorological discrepancies that occur within the tower network by analyzing archived 5-minute tower observations over the past nine years. The task will also result in a tool that forecasters can use to view the results.

### ***Tower Climatology***

Mr. Case completed the quality control of the nine-year tower network database (February 1995 to January 2004) and finished the tower climatology calculations. The tower climatology consists of hourly means, standard deviations, biases, and data counts or percentages of data availability of 6-ft and 54-ft temperatures, the difference in the 54-ft and 6-ft temperatures, 54-ft wind speed, and 54-ft direction deviation at 33 towers. The data were stratified by month and wind direction bins every 45°. Figure 2 shows all towers that were used for the climatology.

The climatological statistics for all parameters and wind direction bins were displayed in Microsoft® Excel® pivot charts and tables, similar to those shown in the previous AMU Quarterly Report (Q1 FY04). However, the final presentation of the pivot charts uses a line-graph format so that results at multiple towers can be overlaid simultaneously. A sample pivot chart that will be available to users is shown in Figure 3.

The climatological results were also analyzed objectively onto a grid in order to generate contour plots of each quantity and wind direction categorization for display in a geographical tool. The mean, standard deviation, and bias results were converted into files compatible with the General Meteorological Package (GEMPAK) software by hour, month, variable, and wind direction bin. The statistical results for each hour, month, variable, and wind direction bin were then analyzed using the two-pass Barnes (1973) algorithm in GEMPAK, as described by Koch et al. (1983). Graphical images were created by overlaying the statistical results with contours. A total of 12,960 images were generated, given all possible permutations (5 parameters x 9 wind direction categories x 12 months x 24 hours).

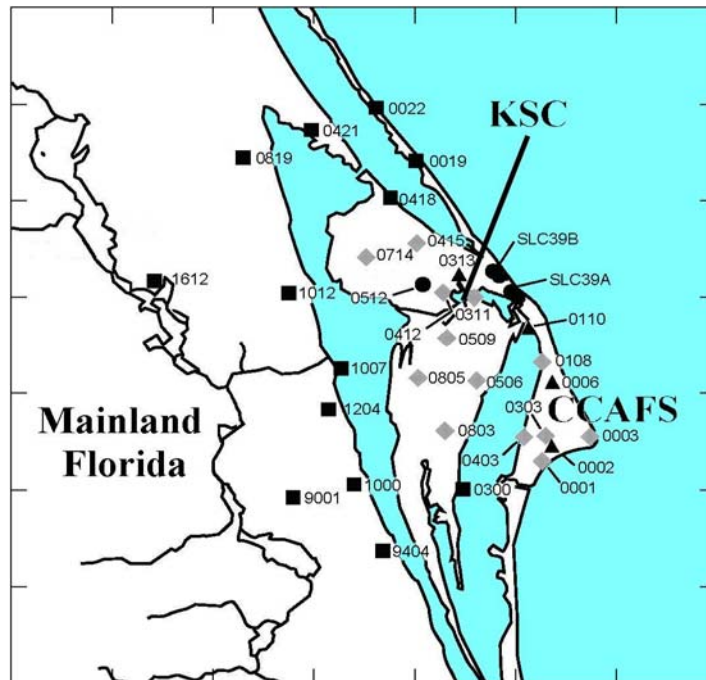


Figure 2. Map of the 33 tower locations and their station numbers used in the nine-year climatology. Black squares are the forecast critical towers, gray diamonds are the safety critical towers, black circles are the launch critical towers, and black triangles are the launch and safety critical towers.

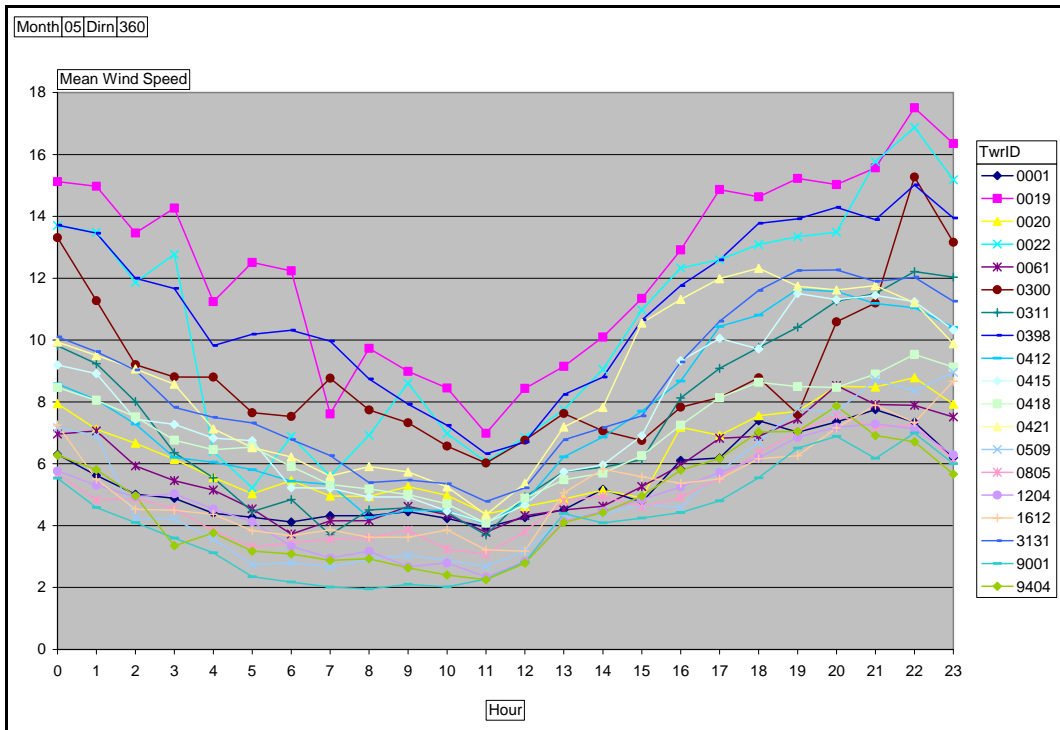


Figure 3. This is a sample Excel pivot chart that will be available to users as part of the final task deliverable. This chart shows the mean hourly wind speed (kts) during May for the wind direction bin ending at 360° (i.e. 315° < Dir ≤ 360°) for the towers listed at the right.

**Graphical User Interface (GUI)**

Dr. Bauman integrated the pivot charts and contoured images into a single graphical user interface (GUI) that will serve as the final task deliverable. He chose a web-based GUI for portability and ease of use. The GUI was written using HTML and JavaScript and can be viewed on computers running various operating systems. Since the pivot charts were created using Microsoft® Excel®, the web browser required to view and interact with the pivot charts is Microsoft® Internet Explorer 5.01 Service Pack 2 or later and Microsoft® Office® 2003 web components plug-in (free download from Microsoft®). The GUI uses a navigation style that allows users to jump between data types and parameters with minimal mouse clicks. When the user starts the GUI they are presented with the main page which contains the main menu as shown in Figure 4. From here, the user can choose to view the pivot charts, maps, or help files.



Figure 4. Main menu of the GUI provides navigation to the pivot charts, maps, or help files.

When the user selects “Pivot Charts” from the main menu, they are presented with two navigation choices on the pivot chart selection page. They can choose to display all months and all wind directions, or view the data stratified by season and wind direction (Fig. 5). A series of other parameters and data set choices are presented to the user so they can navigate to the pivot chart they want to interrogate. An example of the resulting navigation through the GUI with an interactive pivot chart displayed is shown in Figure 6.



Figure 5. The pivot chart selection page provides two navigation choices.

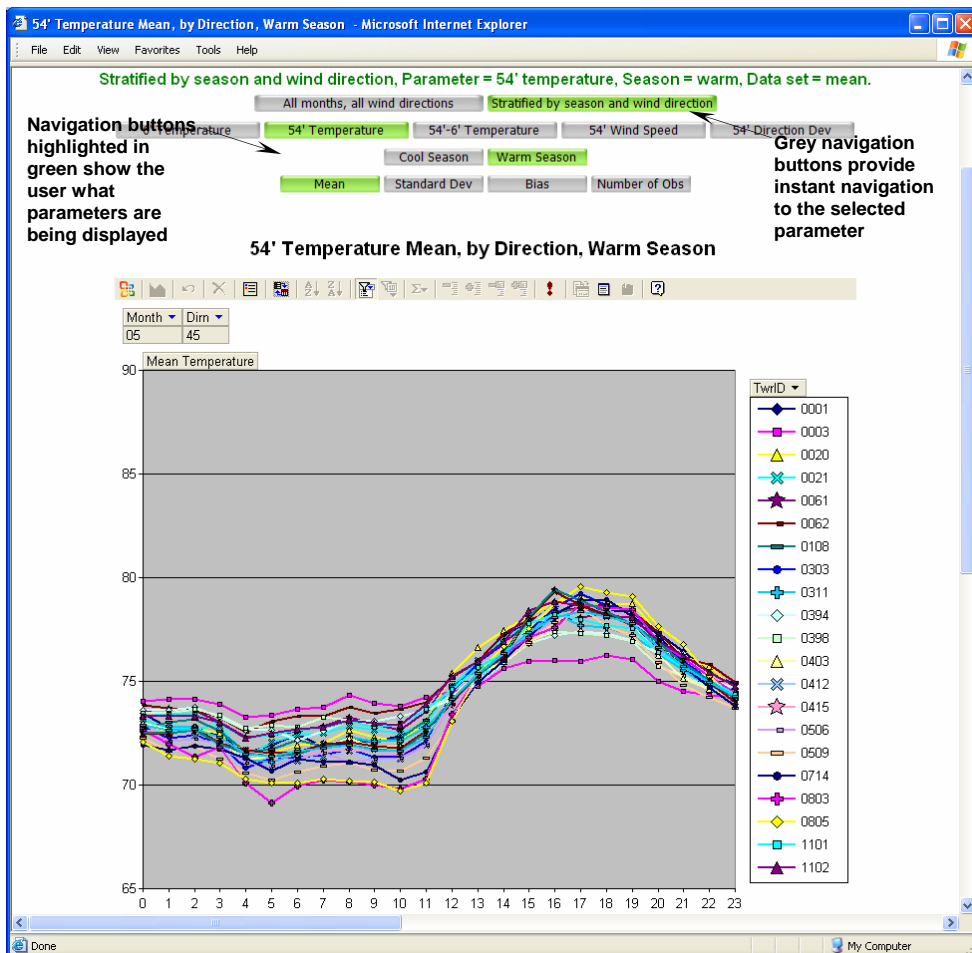


Figure 6. Display of a pivot chart showing the parameters and data sets chosen by the user.

When the user selects “Maps” from the main menu, they are presented with all 12 months on the main maps selection page (Figure 7). A series of other parameters and data set choices are presented to the user so they can navigate to the maps they want to display. An example of the resulting navigation through the GUI with maps displayed is shown in Figure 8.



Figure 7. The maps selection page first provides the user with a choice of month.

In addition to hourly maps, users can choose to loop through all hours for any given month, parameter, and wind direction bin. As shown in Figure 9, loops use an interactive JavaScript animation tool that will continuously loop through all 24 hours of data, “rock” forward and backward through the data, adjust the animation speed, start/stop the animation, move forward or backward one hour at a time, move to the first or last map, and zoom.

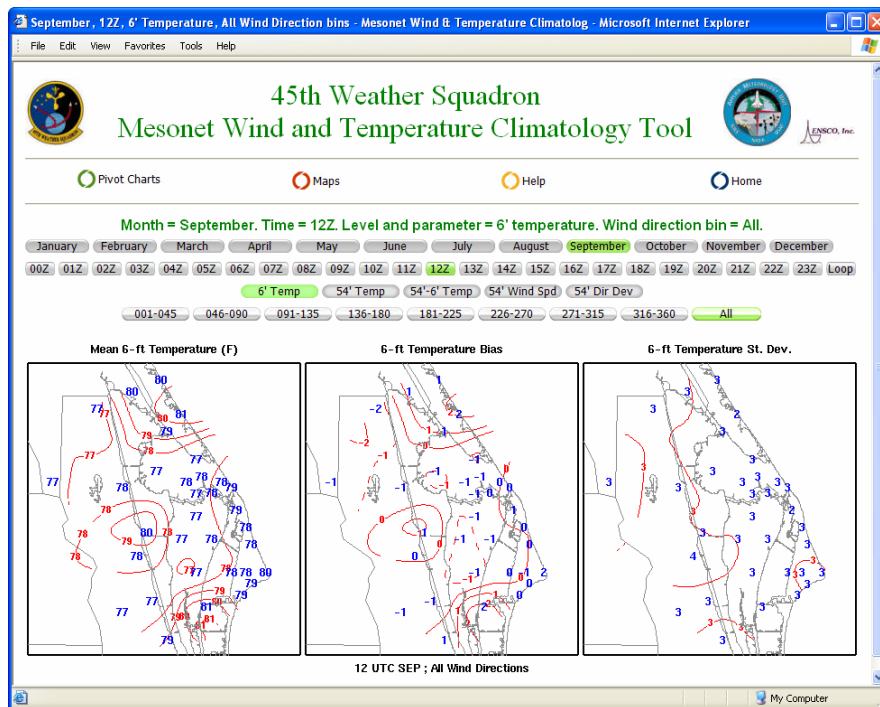


Figure 8. Display of maps showing parameters and data sets chosen by the user.

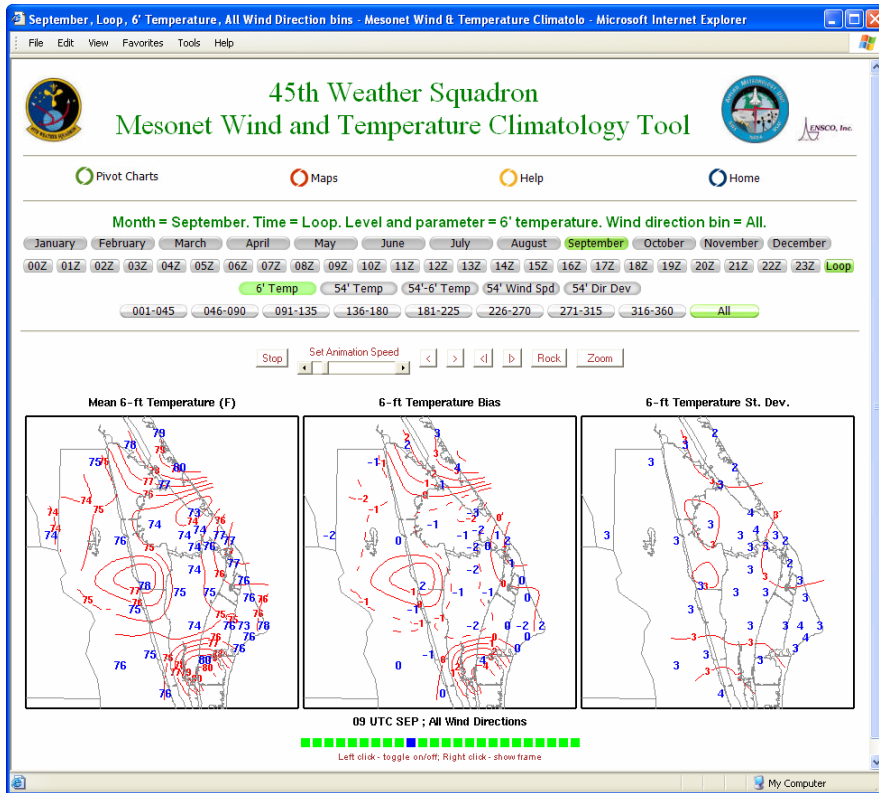


Figure 9. Maps page displaying data with the JavaScript animation tool.

For more information on this work, contact Mr. Case at 321-853-8264 or [case.jonathan@ensco.com](mailto:case.jonathan@ensco.com) or Dr. Bauman at 321-853-8202 or [bauman.bill@ensco.com](mailto:bauman.bill@ensco.com).

#### SEVERE WEATHER FORECAST DECISION AID (MR. WHEELER AND DR. SHORT)

The 45 WS Commander's morning weather briefing includes an assessment of the likelihood of local convective severe weather for the day in order to enhance protection of personnel and material assets of the 45th Space Wing, CCAFS, and KSC. The severe weather elements produced by thunderstorms include tornadoes, wind gusts  $\geq 50$  kts, and/or hail with a diameter  $\geq 0.75$  in. Forecasting the occurrence and timing of these phenomena is challenging for 45 WS operational personnel. The AMU has been tasked with the creation of a new severe weather forecast decision aid, such as a flow chart or nomogram, to improve the various 45 WS severe weather watches and warnings. The tool will provide severe weather guidance for the day by 1100 UTC (0700 EDT).

In a continuing effort to expand the AMU database of severe weather events in east-central Florida and atmospheric stability indices from the daily morning rawinsonde observation (RAOB) at XMR, Mr. Wheeler and Dr. Short requested: 1) Ms. Lambert to extend the computation of stability indices from the XMR rawinsonde into the months of February through April, 2) a local database of severe weather events from the National Weather Service office in Melbourne, FL (NWS MLB), and 3) CSR personnel at XMR to search their archive of rawinsonde data for about 240 observations that are missing in the AMU archive between 1989 - 2003. The first request was motivated by the fact that a substantial fraction of severe weather events observed in east-central Florida occurred during the latter months of the cool season and the transition to the warm season. The second request was motivated by the discovery that the severe weather event of 3 May 1994, documented by NWS MLB personnel (Sharp and Hodanish 1996), did not appear in the National Climatic Data Center (NCDC) database used for the AMU database, for unknown reasons. NWS MLB personnel have also provided the AMU access to additional potential sources of severe weather events within the NCDC database structure. The third request was made to fill in missing days on which severe weather may have occurred.

At the time of this report, the AMU database of east-central Florida severe weather events for the warm seasons of 1989 – 2002 contained 253 severe weather days out of 1902 total days. This database was analyzed to determine the frequency of occurrence of severe weather days when stability indices from the XMR RAOB were within the High, Medium and Low threat categories defined on 45 WS Form 5 (Patrick AFB/SLF Summer Terminal Aerodrome Forecast Worksheet). Table 1 shows the threat categories for Showalter Stability Index (SSI) and the Lifted Index (LI) values. For example, if the SSI is less than -2 and/or the LI is less than -5, there is a high threat of severe storm occurrence.

Table 1. Threshold values of SSI and LI stability indices for the High, Medium, and Low threat categories as found on 45 WS Form 5.			
<i>Index</i>	<i>High</i>	<i>Medium</i>	<i>Low</i>
<b>SSI</b>	< -2	2 to -2	> 3
<b>LI</b>	< -5	-3 to -5	> -2

The SSI provides a measure of the potential instability of the layer between 850 – 500 mb and is used to identify potential areas of thunderstorm development, a prerequisite for severe weather events as defined above. The upper half of Table 2 shows the number of days when the SSI values were within the High, Medium, and Low threat categories and the number of days on which severe weather actually occurred. As an example, the SSI was in the High range (<-2) on 95 of 1902 total days, and severe weather occurred on 25 of those 95 days. The percent occurrence of severe weather when the SSI was < -2, then, is 26.3% (25 out of 95). The Medium threat category was lower at 15.6%, and the Low threat category was the lowest at 8.9%.

The LI is a measure of potential instability between the surface and 500 mb. The lower half of Table 2 shows the number of occurrences for the LI within the High, Medium and Low threat categories. Table 2 indicates that when the LI was in the High Threat range (<-5), the percent occurrence of severe weather was 18.9%, 36 out of 190. The Medium threat category was only slightly lower at 18.2%, and the Low threat category was the lowest at 9.6%.

Table 2. The number of days in which the SSI and LI values were within the High, Medium and Low threat categories, and the number of those days on which severe weather occurred. There is a total of 1902 days in the AMU database. Severe weather occurred on 253 of those days.					
<b>SSI</b>	<i># Days:</i>	<i>High</i>	<i>Medium</i>	<i>Low</i>	<i>Total</i>
	<i>Total</i>	95	1008	799	1902
	<i>Severe</i>	25	157	71	253
	<i>% Severe</i>	26.3%	15.6%	8.9%	13.3%
<b>LI</b>	<i># Days:</i>	<i>High</i>	<i>Medium</i>	<i>Low</i>	<i>Total</i>
	<i>Total</i>	190	609	1103	1902
	<i>Severe</i>	36	111	106	253
	<i>% Severe</i>	18.9%	18.2%	9.6%	13.3%

The analyses of LI and SSI occurrences shown in Table 2 and similar analyses of the K Index and the Total Totals Index will be used to re-assess the threshold values currently used on 45 WS Form 5. If necessary, the AMU will recommend an adjustment of the threshold values based on the historical severe weather events in east-central Florida and the accompanying stability indices from the morning XMR RAOB. The AMU archives of severe weather events, stability indices and synoptic characterizations of atmospheric flow patterns will be merged for further analysis. The objective will be to develop a severe weather decision aid that is tuned to the east-central Florida environment.

For more information on this work, contact Mr. Wheeler at 321-853-8205 or [wheeler.mark@ensco.com](mailto:wheeler.mark@ensco.com), or Dr. Short at 321-853-8105 or [short.david@ensco.com](mailto:short.david@ensco.com).

### **SHUTTLE ASCENT CAMERA CLOUD OBSTRUCTION FORECAST (DR. SHORT AND MR. LANE)**

Optical imaging of the Shuttle launch vehicle (LV) from ground-based and airborne cameras is susceptible to obstruction by clouds. The Columbia Accident Investigation Board (CAIB) recommended that the Shuttle ascent imaging network be upgraded to have the capability of providing at least three useful views of the LV from lift-off to Solid Rocket Booster (SRB) separation. In response, the NASA/KSC Weather Office tasked the AMU to develop a model to forecast the probability that, at any time from launch to SRB separation, at least three of the Shuttle ascent imaging cameras will have a view of the vehicle unobstructed by cloud. The resulting AMU model was based on computer simulations of 1) idealized, random cloud coverage scenarios, 2) the optical lines-of-sight from cameras to the LV using the camera network before and after upgrades for Return to Flight (RTF) and 3) a LV ascent trajectory for a launch from Pad 39B to the International Space Station (ISS).

#### ***Study Design***

The computer simulation model was used to estimate the probability that a network of cameras could obtain at least a certain number (N) of simultaneous views of the Shuttle LV from lift-off to SRB separation in the presence of clouds. The model generated line-of-sight (LOS) data for the camera network and LV ascent trajectory. The camera network and ascent trajectory were embedded in a 3-dimensional (3-D) field of randomly distributed clouds. The LOS from each camera to the LV was computed along its trajectory and cloud obscuration was noted as a binary variable, either obscured or clear. The obscuration data were then analyzed to determine the fraction of time from liftoff to SRB separation that at least N simultaneous views of the LV were obtained by the camera network, where N ranged from 2 to 6. A total of 1000 trials with randomly distributed clouds were analyzed for each of approximately 100 different cloud scenarios. The cloud scenarios had prescribed cloud bases, tops and sizes, with cloud coverage ranging from 1/8 to 7/8.

#### ***Camera Network***

Characteristics of the camera network used in this simulation study were obtained from Mr. Robert Page, Chair of the Intercenter Working Photo Group (IWPG), at NASA/KSC and Mr. Robbie Robinson, a member of the IWPG. Required characteristics were confined to camera locations and the portion of the ascent trajectory where high-resolution imagery of the LV can be obtained by each of three camera types: short-range, medium-range and long-range. A detailed description of the camera network can be found in Bauman (2003). Figure 10 shows the long-range cameras after upgrade along with the ground track of the ascent trajectory for an ISS mission, out to SRB separation.

There are numerous short-range and medium-range tracking cameras located around the Shuttle launch pads. These provide high-resolution imagery from a few seconds before lift-off until the LV reaches an altitude of ~7000 ft, ~26 seconds after lift-off. The short-range cameras were not included in the simulation results presented here because their range is limited to ~1500 ft and the cloud coverage scenarios did not include clouds with bases below 1500 ft. It was assumed that the medium-range cameras picked up where the short-range cameras left-off, acquiring the required imagery until the LV reached ~7000 ft. The LV reaches 7000 ft in ~26 sec, which is 21 % of the total time from lift-off to SRB separation.

The camera sites are designated as north or south depending on whether their view of the ascent trajectory is from the north or south side. After the LV completes its roll maneuver to a belly-up, heads-down position, about 10 seconds after lift-off, the right side of the LV is viewable from the north side cameras, while the left side of the LV is viewable by the south side cameras. The north and south designations play a role in the analysis of N simultaneous views. For example, the probability of at least 3 simultaneous views of the LV from both sides should be lower than that of at least 3 simultaneous views from the north side. Note in Figure 10 that there are 5 ground-based, long-range camera sites on each of the north and south sides.

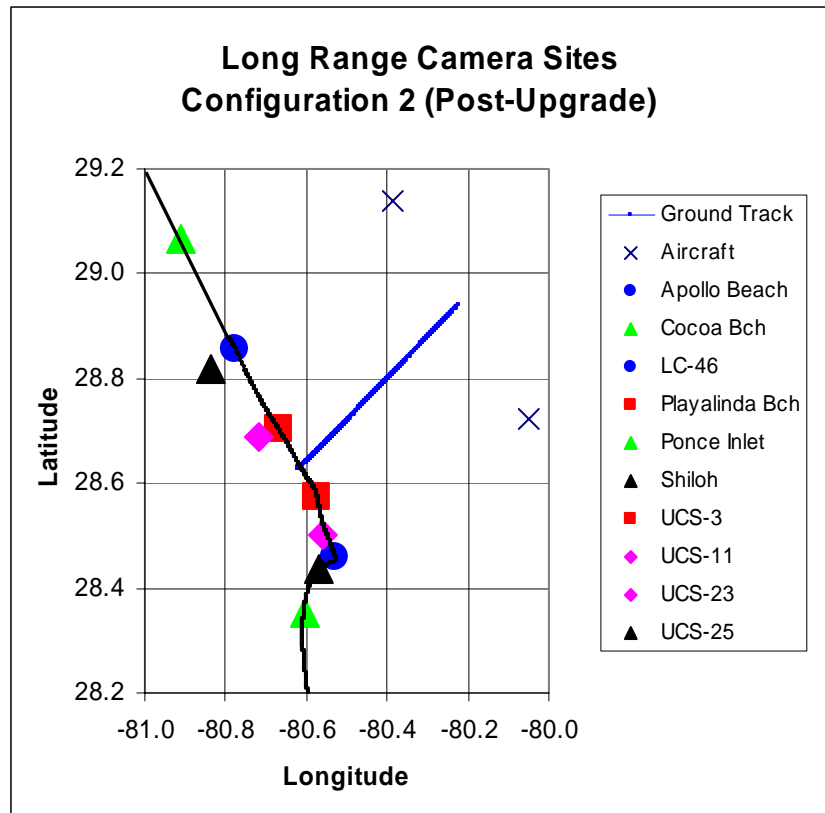


Figure 10. Post-upgrade configuration of the long-range camera sites. The airborne cameras are at 65 000 ft located 15 n mi NE and SW of the SRB separation point.

### *Line-of-Sight*

The LOS from a tracking camera to the LV sweeps across the sky as the LV travels along its ascent trajectory. Figure 11 shows an imaginary 3-D surface made up of sequential LOSs from one camera, located at upper left, to the LV from lift-off to SRB separation at 155 000 ft. The 3-D surface is divided into regions A, B, and C, where the boundaries have been determined by a cloud base altitude (CB) and a cloud top altitude (CT). If cloud elements were present within region C they would obscure the LOS from the camera to the LV sometime during its ascent. Similar cloud elements within region A could not obscure the view as the LOS would pass beneath them during the portion of the ascent from lift-off until the LV reached cloud base. In a similar manner cloud elements in region B could not obscure the LOS as it and the LV would be above them and they would be too far from the camera site.

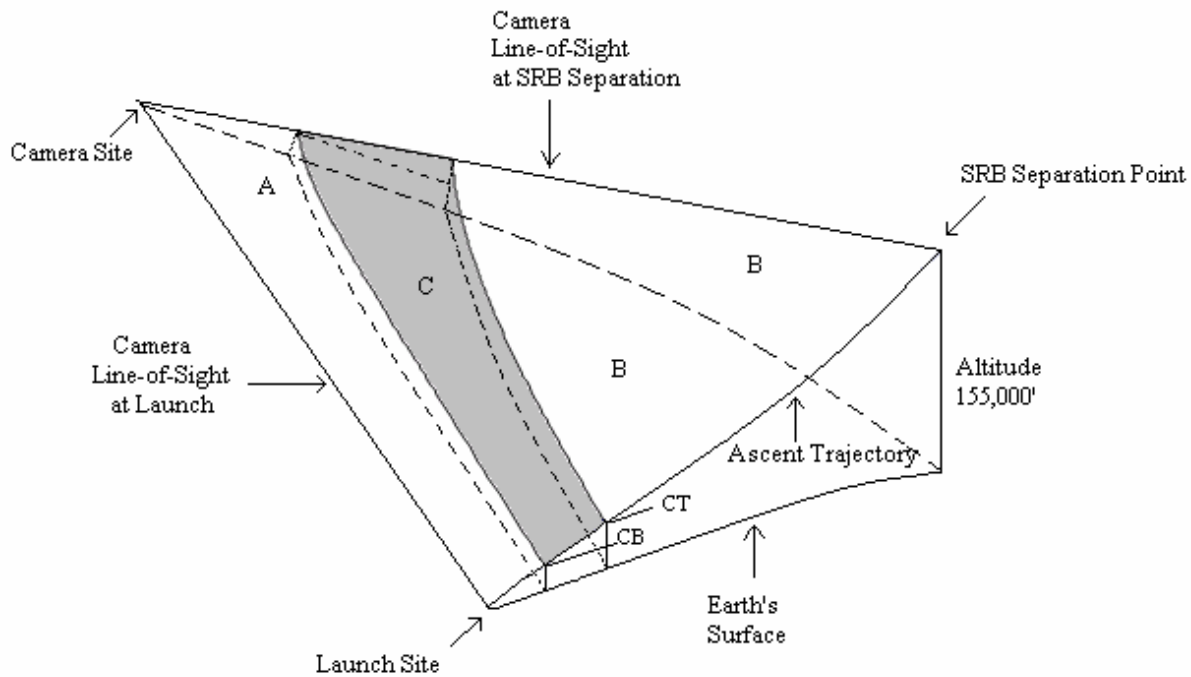


Figure 11. Schematic view of the LOSs from a camera site in the upper left-hand corner to an LV along its ascent trajectory from lift-off at the launch site to SRB separation, 155 000 ft above the Earth's surface. Regions A, B, and C comprise a 3-D surface of the LOSs from the camera to the LV along its ascent trajectory. Region C is the domain where cloud elements with bases at altitude CB and tops at altitude CT have the potential for obscuring the LOS from the camera to the LV during its ascent.

The geographic boundaries of region C in Figure 11 can be computed for any camera site and any prescribed CB and CT. Figure 12 shows a composite of the zones susceptible to cloud obscuration for the long-range camera network shown in Figure 10 with cloud bases at 3,000 ft and cloud tops at 27 000 ft. This cloud scenario could be representative of late morning convective elements during the warm season (May – September) or frontal clouds during the cool season (October – April). The zones susceptible to cloud obscuration shown in Figure 12 are mostly offshore and are confined to within less than 10 n mi of the coast.

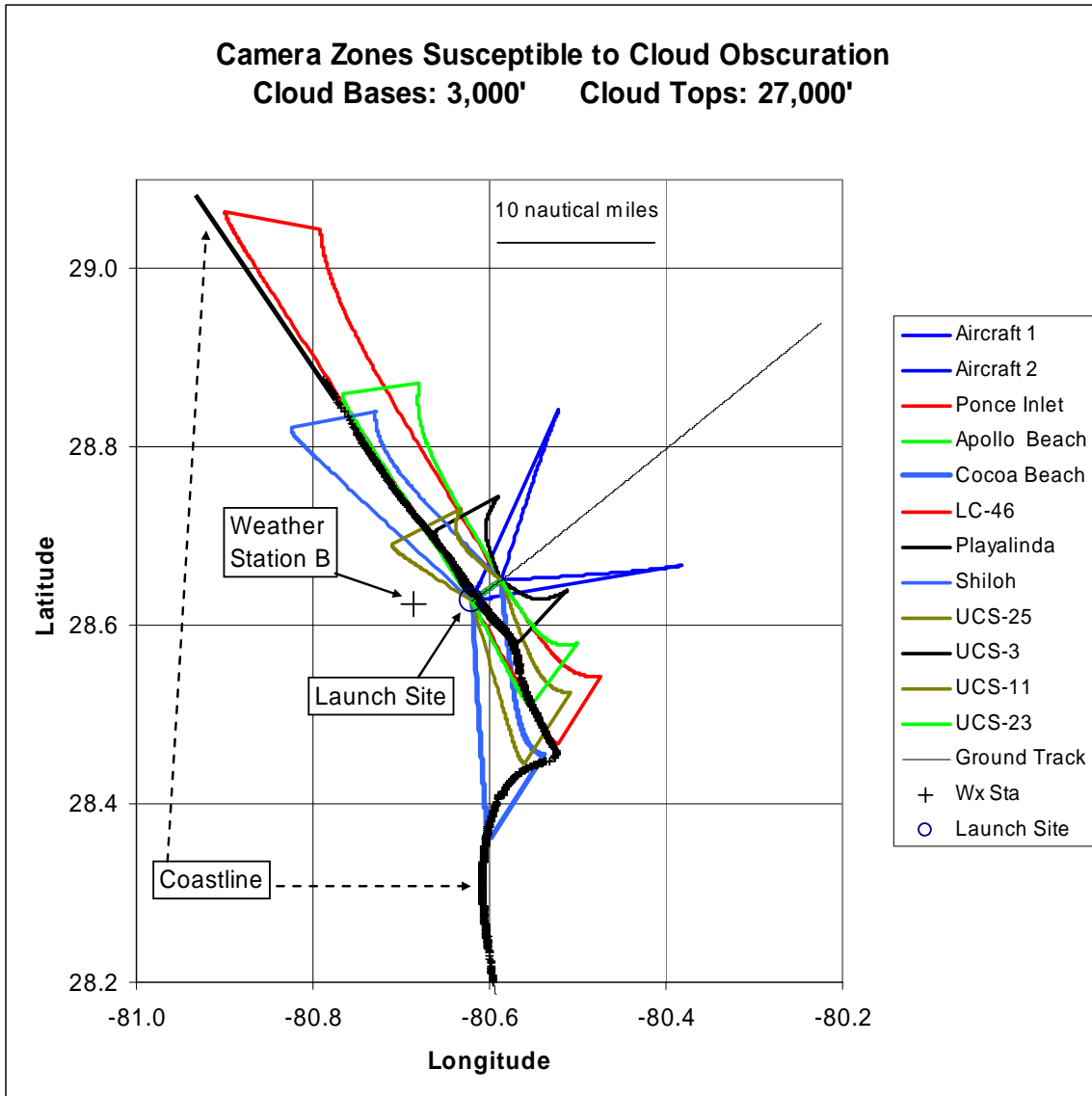


Figure 12. Geographical pattern of camera zones susceptible to cloud obscuration for the upgraded long-range camera network with cloud bases at 3000 ft and cloud tops at 27 000 ft. Weather Station B near the SLF (+) is where routine surface-based observations of cloud base height and cloud amount are obtained.

The complex geographical pattern shown in Figure 12 is indicative of the difficult challenges to providing an accurate, deterministic forecast of the effect of clouds on viewing conditions from a network of cameras. Although it may be possible to map out the current cloud geometry over the region with advanced instrumentation such as cloud radars, cloud lidars and high-resolution satellite observations (Bauman 2003), an accurate 15-minute forecast of the cloud geometry would be even more challenging.

#### ***Viewing Probability***

Model output was analyzed from each of 1000 trials of a given cloud scenario to determine the fraction of time from lift-off to SRB separation that the LV was viewable simultaneously by at least N cameras. N was varied from 2 to 6. The probability of at least N-simultaneous views of the LV was computed as the average percentage over the 1000 trials. The average percentages were computed for cloud coverages ranging from clear (0/8) to overcast (8/8) every 1/8.

Figure 13 shows fractional cloud coverage versus the percentage of time from lift-off to SRB separation that the LV was viewable simultaneously from both the north and south sides by at least 1, 2, and 3 cameras. A mid-level cloud base at 8000 ft was chosen for this scenario because of existing weather LCC. The weather LCC for Shuttle ceiling rules would be GO for a ceiling at 8000 ft. Figure 13 indicates that the percent of time viewable simultaneously by at least three cameras from both the north and south side (six total cameras) decreased rapidly as cloud cover increases beyond 1/8. At the point where cloud cover reaches 5/8, constituting a ceiling, the percent viewable factor has decreased to less than 50% (80%) for 3 (2) cameras. The percent of time viewable for two and three simultaneous views decreased to 22.4% for overcast conditions, corresponding to the time when the LV entered cloud base. For the case of simultaneous single views from the north and south sides the airborne cameras contributed significantly and the drop to 77.5% under overcast conditions corresponded to the time the LV spent above cloud tops.

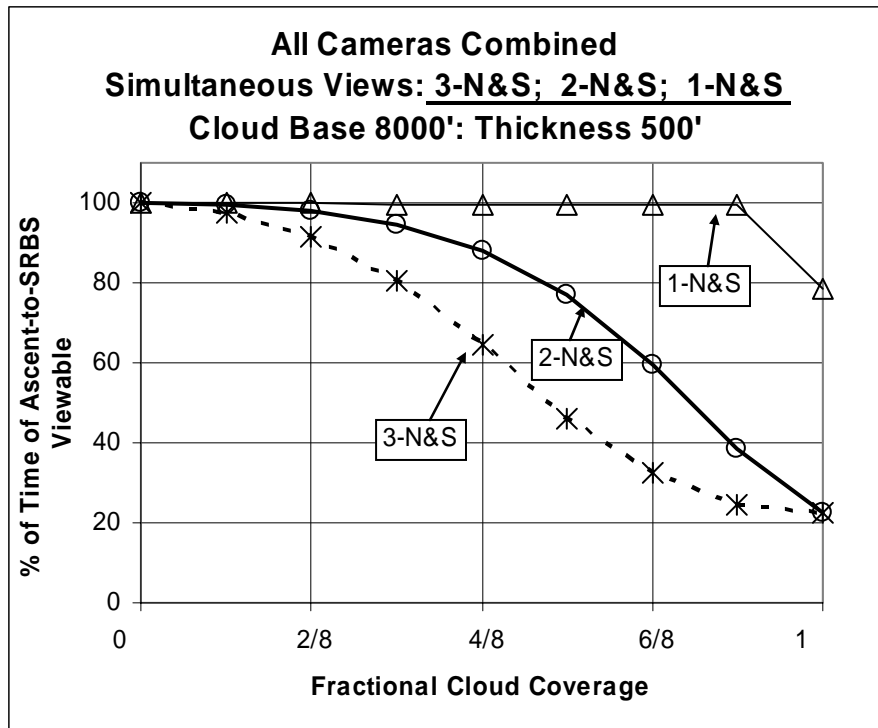


Figure 13. Fractional cloud cover versus percent of time from lift-off to SRB separation that the LV was viewable simultaneously from both the north and south sides by at least 1, 2, and 3 cameras.

For more information on this work, contact Dr. Short at 321-853-8105 or [short.david@ensco.com](mailto:short.david@ensco.com), or Mr. Lane at 321-783-9735 Ext. 245 or [lane.bob@ensco.com](mailto:lane.bob@ensco.com).

## **INSTRUMENTATION AND MEASUREMENT**

### **I&M AND RSA SUPPORT (MR. WHEELER AND DR. BAUMAN)**

Mr. Wheeler continued evaluating, testing and developing new procedures for the RSA Advanced Weather Interactive Processing System (AWIPS) display system. A new AWIPS release, Operational Build 1 (OB1) was installed and tested by Lockheed Martin (LM) and Forecast Systems Laboratory personnel. After it was installed, Mr. Wheeler tested OB1 the system using the standard procedures and some he had developed previously. He noticed a slow-down in performance of the AMU's AWIPS system during testing. He noted the issue in the AMU's log book and relayed the information to LM personnel. Mr. Wheeler also noticed that the NWS MLB Weather Surveillance Radar 88 Doppler (WSR-88D) data was no longer part of the Florida radar composite image. Mr. Russ Bolton of LM created a temporary fix to the problem until a permanent solution can be engineered.

## **ANVIL TRANSPARENCY RELATIONSHIP TO RADAR REFLECTIVITY (DR. SHORT AND MR. WHEELER)**

Determining the transparency of anvil clouds is critical for the operational evaluation of FR and LCC. A non-transparent anvil that is attached to the parent thunderstorm is likely to be electrically charged and could subject a launch vehicle or landing Shuttle to natural and/or triggered lightning. Forecasters currently rely on satellite observations, pilot reports and surface based observations to determine if anvil clouds are non-transparent, which is a violation of LCC and FR if the flight path of a vehicle would pass through such clouds. However, these types of cloud observations are not always available, depending on the location of the anvil clouds, the presence of other cloud layers and the time of day. The WSR-88D at NWS MLB provides high-resolution cloud reflectivity information over the KSC/CCAFS area on a continuous basis. Routine products from the WSR-88D could be useful for determining anvil transparency and are available in real-time at SMG and the 45 WS Range Weather Operations. One of those products identified by SMG is the Layered Reflectivity Max (LRM) High product, which determines the maximum reflectivity value in the 33 000 – 60 000 ft layer. The AMU was tasked to determine if the WSR-88D LRM High product would be useful in evaluating anvil transparency.

In this study, LRM High product data will be analyzed along with surface observations of thunderstorm anvil transparency over Weather Station B (KTTS) at the SLF to determine if there is a threshold LRM High value to distinguish between transparent and opaque anvils. The period of record for the study is the warm season (May – September) of 2003. The AMU made a special request that the observers at KTTS record the cirrus anvil transparency. They determined the transparency of cirrus overhead but could not distinguish whether the cirrus were from thunderstorm anvils or not. In order to reduce the total amount of data processing and to assure that the analysis is confined to thunderstorm anvil clouds only, Mr. Wheeler used a two-step filtering approach. First, he examined the KTTS observations to find days with several continuous hours of remarks on opaque and thin cirrus overhead. In the second step, he used visible satellite imagery to identify case days where the cirrus referred to in the KTTS remarks had clearly originated from thunderstorm activity. Mr. Wheeler collected hourly Geosynchronous Operational Environmental Satellite (GOES) visible satellite images from an AMU archive for days with reports of thin and opaque cirrus overhead at KTTS. He then identified 45 days with satellite-indicated anvil cirrus in the vicinity of KSC/CCAFS and remarks indicating transparent/opaque cirrus overhead in the KTTS surface observations.

Figure 14 provides an example of how Mr. Wheeler carried out the second step in the filtering process. It shows a set of visible satellite images from 8 July 2003, one of the 45 days in the final data set. Standard and grey-scale enhanced images are shown for 2000 and 2045 UTC (1600 and 1645 EDT). The visible grey-scale enhancement was used in an earlier study of the lifetime and propagation characteristics of thunderstorm anvil clouds over east-central Florida (Short et al. 2002). At 2000 UTC (Fig. 14a and b) a veil of anvil cloud originating from thunderstorms over the ocean covered the KSC/CCAFS area. The enhanced image on the upper right shows that the clouds over the KSC/CCAFS area were bright white, suggesting that they were opaque and consistent with remarks in the KTTS observation. At 2045 UTC (Fig. 14d) the bright white anvil cloud cover shifted southward and, again, was consistent with the KTTS observation of transparent cirrus overhead at the same time.

Mr. Wheeler downloaded the corresponding WSR-88D Level-II radar data from NWS MLB from NCDC. He also found and acquired several software packages that display Level-II data. He installed and tested all programs found on one of the AMU UNIX workstations, but found that none of the programs allowed development of the LRM High product needed for the task. Through further research he found that the NCDC archives include products derived from the WSR-88D network, including the LRM High image. Mr. Wheeler contacted Mr. Tim Crum of the NOAA Radar Operations Center and asked if there was software available to display the archived LRM High data. Mr. Crum offered to have his staff develop the images if the AMU provides the dates and times needed.

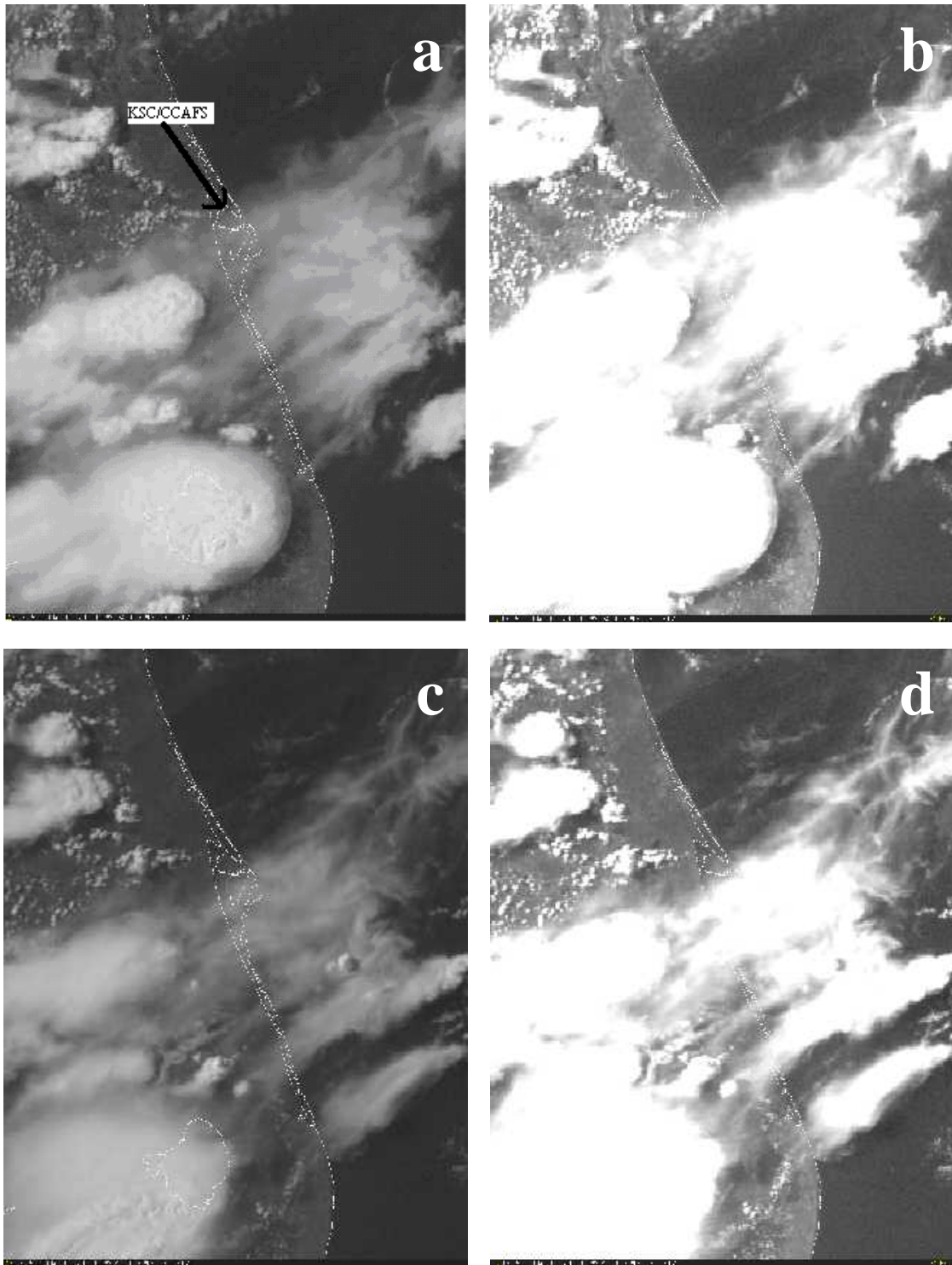


Figure 14. Visible satellite imagery of non-transparent and transparent anvil clouds over the KSC/CCAFS area on 8 July 2003. The 2000 UTC visible image is shown with standard (a) and low-light enhancement (b) grey-scales. The enhancement is used to highlight the transition between non-transparent and transparent cirrus. The 2045 UTC visible image with standard (c) and enhanced (d) grey-scales.

### *Theoretical Considerations*

Microphysical characteristics of cirrus clouds affect their optical transparency (Platt 1997) and their radar reflectivity (Sassen 1987). Sassen (1987) provides an approach for estimating the mass content of ice clouds (Mi) given observations of the radar equivalent reflectivity factor (dBZe), and Platt (1997) provides a method for using Mi to estimate the visible extinction coefficient ( $\sigma$ ). The optical thickness ( $\tau$ ) can then be obtained by the product of  $\sigma$  and the geometric thickness ( $\Delta Z$ ). The following algorithmic approach was used to estimate  $\tau$  from dBZe:

- 1) Compute  $Z_e = 10^{(\text{dBZe}/10)}$
- 2) Compute  $Z_i = 5.28 \times Z_e$
- 3) Compute  $M_i = 0.017 \times Z_i^{0.529}$
- 4) Compute  $\sigma = 5.48 \times M_i^{0.54}$
- 5) Compute  $\tau = \sigma \times \Delta Z$

The conversion from  $Z_e$  to  $Z_i$  in 2) accounts for differences in the complex indices of refraction between ice and water, because the radar equation used in standard radar systems assumes the targets are water (rain) droplets (Sassen 1987). The coefficients in 3) were obtained from Sassen's (1987) parameterization of Heymsfield and Palmer's (1986) microphysical data from thunderstorm anvil clouds. The coefficients in 4) were obtained from Platt's parameterization of Heymsfield and Platt's (1984) microphysical data. Although it would be desirable to have a completely self-consistent set of microphysical data from anvil clouds to develop similar parameterizations for the estimation of  $\tau$ , the approach outlined above and the preliminary results shown below provide some insight into the dependence of  $\tau$  on dBZe and  $\Delta Z$ .

Figure 15 shows the estimated optical thickness ( $\tau$ ) of anvil cirrus given the radar equivalent reflectivity factor (dBZe) and the geometric thickness ( $\Delta Z$ ) as computed via equations 1) through 5) above. For a dBZe value near 10 and a  $\Delta Z$  corresponding to 10 000 ft (bold lines), Figure 15 shows a value of  $\tau$  near 6. This value is significant because it corresponds to the optical thickness required to obscure bright stars from the view of a human observer at the surface. Recall that one criterion used in the determination of anvil transparency is whether or not stars are visible through the cloud. Under ideal conditions a human observer can see stars with an apparent brightness of magnitude  $\sim +6$  with the naked eye, and the brightest stars that appear overhead in the KSC area have magnitudes near +1. An increase in magnitude corresponds to a logarithmic decrease in brightness: a star with magnitude +6 is  $\sim 1/100$  the brightness of a magnitude +1 star. The optical thickness of a cloud has approximately the same effect on the brightness of an object by only allowing a fraction of the light to pass through. A cloud with  $\tau = 4.6$  would only allow 1/100 of the light from an object to pass through. Therefore, a cloud with an optical thickness of 6 would diminish the light of a star with a brightness magnitude of +1 by more than 1/100, and a human observer would thus judge the cloud to be non-transparent.

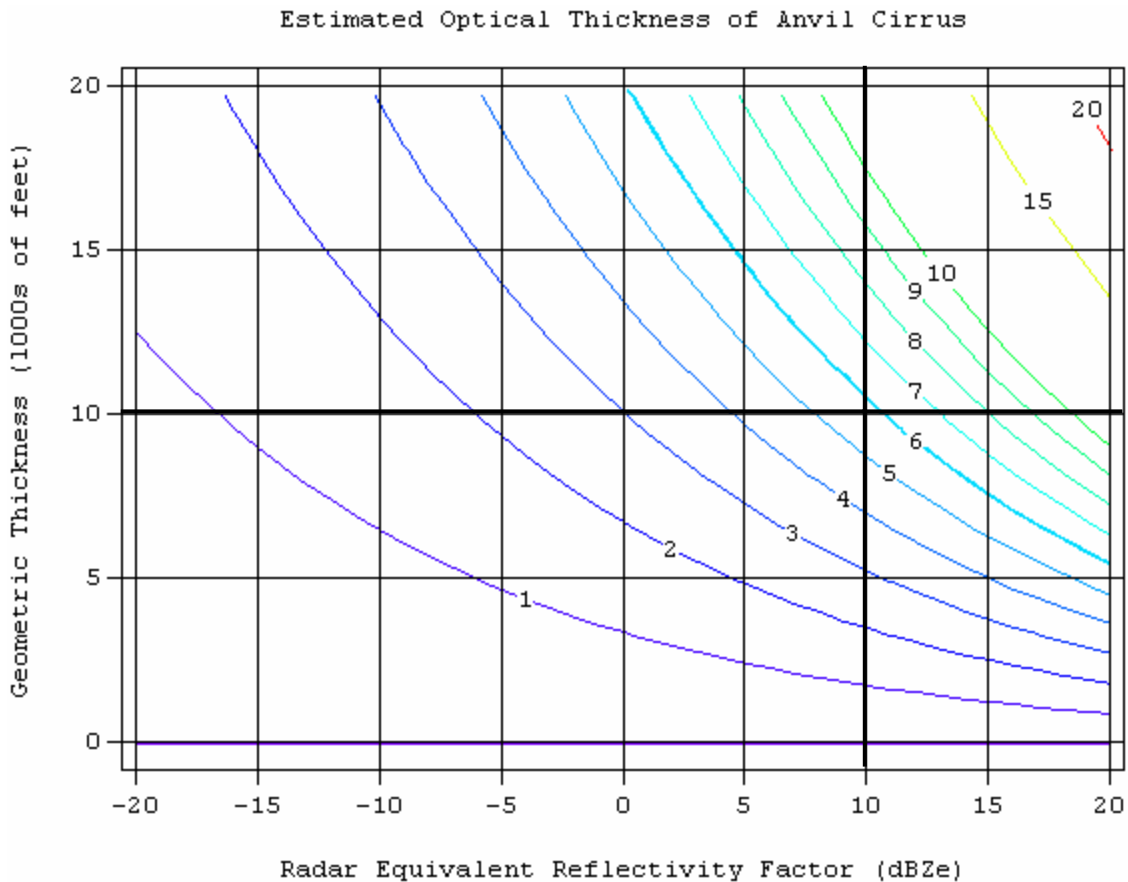


Figure 15. Estimated optical thickness of anvil cirrus given the radar equivalent reflectivity factor (dBZe) and the geometric thickness (1000s of feet). The algorithm is based on idealized parameterizations of ice crystal size distributions described in the text. The bold lines at 10 dBZe and 10 000 ft highlight the example in the text.

For more information on this work, contact Dr. Short at 321-853-8105 or [short.david@ensco.com](mailto:short.david@ensco.com), or Mr. Wheeler at 321-853-8205 or [wheeler.mark@ensco.com](mailto:wheeler.mark@ensco.com).

**AMU CHIEF'S TECHNICAL ACTIVITIES (DR. MERCERET)**

Dr. Merceret presented an overview of upper air wind behavior and measurement techniques to personnel from the Western Range at the request of the Titan Program. He also completed major upgrades to software that analyzes data collected during the Airborne Field Mill campaign, and began work on a comparative analysis of candidate radar variables for revised lightning LCC.

**AMU OPERATIONS**

Mr. Wheeler continued working with the NASA Procurement Office on the AMU IT hardware and software requirements for FY 2004. Most of the AMU's software and hardware IT requirements have been submitted to the NASA Procurement Office.

Dr. Bauman attended the 84th AMS Annual Meeting in Seattle, WA. He also attended the 2nd SMG Weather Users Forum at Johnson Space Center and co-presented (with Ms. Kathy Winters, 45WS Shuttle LWO) Dr. Short's and Mr. Lane's work on the Shuttle Ascent Camera Cloud Obstruction Forecast task.

All AMU personnel were involved in writing responses to new task proposals submitted by the 45 WS, SMG, and NWS MLB in preparation for the annual AMU Tasking Meeting on 10 February. All AMU personnel also attended the meeting. Several new tasks were approved for the coming year. All AMU personnel wrote task plans outlining the work to be done on each of the new tasks. The following table lists summaries of the new tasks.

<i>Task Name</i>	<i>Product Sought</i>	<i>Operational Benefit</i>	<i>Target Begin Date</i>	<i>Target End Date</i>
User Control Interface for ADAS Data Ingest	–A GUI interface that gives forecasters control of data input and certain model parameters	–Forecaster control of data input allows for quick response to situational needs (bad data, etc.)	Jul 04	Jun 05
ADAS/ARPS Optimization and Training Extension	–Ingest new observational data sets –Assist in porting ADAS code to LINUX workstation –Assist in ARPS upgrade to V5.x –Assist in transition to using RUC model input for ARPS/ADAS –Examine warm-season convection cases to advise on ARPS parameter modifications	–An up-to-date data analysis and forecasting system whose parameters for convection and other meteorological phenomena are tuned to the local environment	Jul 04	Sep 05
Assess AWIPS WSR-88D Fidelity	–A comparison of the frequency and severity of differences between the RWO and NWS MLB AWIPS Level III data	–Knowledge of the RWO AWIPS Level III product accuracy for launch support and weather warning/watch advisories	Jul 04	Jun 05
Hail Index	–An evaluation of current 45 WS hail forecasting techniques –A new hail forecasting tool that provides probability of hail occurrence and the likely size	–A quantitative analysis of the performance of the current hail forecasting tools –Better hail forecasting ability if an improved tool is developed	Apr 04	Sep 05
RSA/Legacy Sensor Comparison	–Ultimately, a comparison between the RSA and legacy temperature, dew point, and wind sensors –This task is data collection only, for one year	–An understanding of the biases between the two sets of instruments and the magnitude of those biases, if any	Apr 04	Mar 05
Mesoscale Model Phenomenological Verification Evaluation	–A list and summary of any existing model phenomenological verification techniques and a determination of whether they can be incorporated into AWIPS	–Knowledge of existing phenomenological techniques and if they can be transitioned to operations	Jul 04	Sep 05
Expanded Tower Statistics for Edwards AFB and Northrup Strip	–Consultation to MSFC personnel who will be conducting the work: – Data quality control – Data stratifications and statistics calculations – GUI development	–Improved wind forecasting at Edwards AFB and Northrup Strip through use of wind climatologies and probability of occurrence of peak winds	Jul 04	Jun 05
Stable Low Cloud Forecast	–Analysis of archived rapidly developing stable low cloud cases to include onset/dissipation times, location, and associated weather regimes	–Improved understanding of stable low cloud climatology and the factors that cause them to form –Improved forecasts of low clouds for Shuttle landings	Jul 04	Sep 05
Meteorological Techniques and State of Science Research	–Updates on current research and forecast tool development that could be useful to weather operations	–Operational customers will be kept up-to-date on latest research –Exchange of ideas for new AMU tasks or procedures on current tasks	Apr 04	Mar 05

## **REFERENCES**

- Barnes, S. L., 1973: Mesoscale objective analysis using weighted time-series observations. NOAA Tech. Memo. ERL NSSL-62, National Severe Storms Laboratory, Norman, OK, 73069, 60 pp. [NTIS COM-73-10781].
- Bauman, W. H., III, 2003: Shuttle Imaging Weather Evaluation Concept Study. Applied Meteorology Unit Memorandum, 36 pp. [Available from ENSCO, Inc., 1980 N. Atlantic Ave., Suite 230, Cocoa Beach, FL, 32931.]
- Heymtsfield, A. J., and A. G. Palmer, 1986: Relations for deriving thunderstorm anvil mass for CCOPE storm water budget estimates. *J. Clim. Appl. Meteor.*, **25**, 691-702.
- Heymtsfield, A. J., and C. M. R. Platt: 1984: A parameterization of the particle size spectrum of ice clouds in terms of the ambient temperature and the ice water content. *J. Atmos. Sci.*, **41**, 846-855.
- Insightful Corporation, 2000: *S-PLUS@6 User's Guide*, Insightful Corp., Seattle, WA, 470 pp.
- Koch, S. E., M. DesJardins, and P. J. Kocin, 1983: An interactive Barnes objective map analysis scheme for use with satellite and conventional data. *J. Appl. Meteor.*, **22**, 1487-1503.
- Lazzara, M. A., J. M. Benson, R. J. Fox, D. J. Laitsch, J. P. Rueden, D. A. Santek, D. M. Wade, T. M. Whittaker, and J. T. Young, 1999: The Man computer Interactive Data Access System (McIDAS): 25 Years of Interactive Processing. *Bull. Amer. Meteor. Soc.*, **80**, 271 – 284.
- Platt, C. M. R., 1997: A parameterization of the visible extinction coefficient of ice clouds in terms of the ice/water content. *J. Atmos. Sci.*, **54**, 2083-2098.
- Sassen, K., 1987: Ice cloud content from radar reflectivity. *J. Clim. Appl. Meteor.*, **26**, 1050-1053.
- Sharp, D., and S. Hodanish, 1996: A survey of supercells over east central Florida: Documentation of the 03 May 1994 severe weather episode. Preprints of the 18th Conference on Severe Local Storms. Feb. 19-23, 1996, San Francisco, 335-339.
- Short, D. A., J. E. Sardonía, W. C. Lambert, and M. M. Wheeler, 2002: Propagation and lifetime characteristics of thunderstorm anvil clouds over Florida. Preprints of the 18th International Conference on Interactive Information and Processing Systems (IIPS) for Meteorology, Oceanography and Hydrology, Orlando, FL, 13 - 18 January 2002, pages 19 - 21.

## List of Acronyms

30 SW	30th Space Wing
30 WS	30th Weather Squadron
45 RMS	45th Range Management Squadron
45 OG	45th Operations Group
45 SW	45th Space Wing
45 SW/SE	45th Space Wing/Range Safety
45 WS	45th Weather Squadron
AFSPC	Air Force Space Command
AFWA	Air Force Weather Agency
AMU	Applied Meteorology Unit
AWIPS	Advanced Weather Interactive Processing System
CAPE	Convective Available Potential Energy
CB	Cloud Base
CCAFS	Cape Canaveral Air Force Station
CIN	Convective INhibition
CGLSS	Cloud-to-Ground Lightning Surveillance System
CSR	Computer Sciences Raytheon
CT	Cloud Top
EDT	Eastern Daylight Time
EL	Equilibrium Level
FR	Flight Rules
FSL	Forecast Systems Laboratory
FSU	Florida State University
FY	Fiscal Year
GEMPAK	General Meteorological Package
GUI	Graphical User Interface
IWPG	Intercenter Working Photo Group
JSC	Johnson Space Center
KSC	Kennedy Space Center
KTTS	Weather Station B Identifier
LCC	Launch Commit Criteria
LCL	Lifted Condensation Level
LFC	Level of Free Convection
LI	Lifted Index
LOS	Line-Of-Site
LRM	Layered Reflectivity Max
LV	Shuttle Launch Vehicle
McIDAS	Man-computer Interactive Data Access System
MIDDS	Meteorological Interactive Data Display System
MSFC	Marshall Space Flight Center
NASA	National Aeronautics and Space Administration
NCAR	National Center for Atmospheric Research
NCDC	National Climatic Data Center
NOAA	National Oceanic and Atmospheric Administration
NSSL	National Severe Storms Laboratory
NWS MLB	National Weather Service in Melbourne, FL
PC	Personal Computer
QC	Quality Control

RAOB	Rawinsonde Observation
RSA	Range Standardization and Automation
SLF	Shuttle Landing Facility
SMC	Space and Missile Center
SMG	Spaceflight Meteorology Group
SRB	Solid Rocket Booster
SRH	NWS Southern Region Headquarters
SSI	Showalter Stability Index
USAF	United States Air Force
WSR-88D	Weather Surveillance Radar 88 Doppler
UTC	Universal Coordinated Time
WWW	World Wide Web
XMR	CCAFS Sounding Identifier

## Appendix A

AMU Project Schedule				
30 April 2004				
AMU Projects	Milestones	Scheduled Begin Date	Scheduled End Date	Notes/Status
Objective Lightning Probability Phase I	Literature review and data collection/QC	Feb 03	Jun 03	Completed
	Statistical formulation and method selection	Jun 03	Oct 03	Delayed Due to Data Collection and McIDAS/HUGE Code Interpretation
	Equation development, tests with verification data and other forecast methods	Aug 03	Nov 03	Delayed as above (Apr 04)
	Develop operational products	Nov 03	Jan 04	Delayed as above (May 04)
	Prepare products, final report for distribution	Jan 04	Mar 04	Delayed as above (Jun 04)
Mesonet Temperature and Wind Climatology	Process data and calculate climatology of biases/deviations	Jul 03	Feb 04	Completed
	Develop tabular and geographical displays	Feb 04	Apr 04	On Schedule
	Final Report	Apr 04	Jun 04	On Schedule
	Assistance in transitioning product into operations	Jul 04	Jul 04	On Schedule
Severe Weather Forecast Tool	Local and national NWS research, discussions with local weather offices on forecasting techniques	Apr 03	Sep 03	Completed
	Develop database, develop decision aid, fine tune	Oct 03	Apr 04	On Schedule
	Final report	May 04	Jun 04	On Schedule
Shuttle Ascent Camera Cloud Obstruction Forecast	Develop 3-D random cloud model and calculate yes/no viewing conditions from optical sites for a shuttle ascent	Jan 04	Jan 04	Completed
	Analyze optical viewing conditions for representative cloud distributions and develop viewing probability tables	Feb 04	Feb 04	Completed

AMU Project Schedule				
30 April 2004				
AMU Projects	Milestones	Scheduled Begin Date	Scheduled End Date	Notes/Status
Shuttle Ascent Camera Cloud Obstruction Forecast (continued)	Memorandum	Feb 04	Mar 04	Delayed to Provide Support for Program Requirements Control Board Briefing
Anvil Transparency Relationship to Radar Reflectivity	Literature search and identification of days with anvil cloud over weather station B near the SLF	Nov 03	Dec 03	Completed
	Analysis of WSR-88D and satellite data for anvil days	Jan 04	May 04	On Schedule
	Memorandum	Jun 04	Jul 04	On Schedule
ARPS Optimization and Training	Assistance for testing and optimizing the real-time ARPS configuration	Jul 03	Dec 03	Completed
	Final task memorandum and training/maintenance manual	Dec 03	Feb 04	Completed

## **NOTICE**

Mention of a copyrighted, trademarked, or proprietary product, service, or document does not constitute endorsement thereof by the author, ENSCO, Inc., the AMU, the National Aeronautics and Space Administration, or the United States Government. Any such mention is solely for the purpose of fully informing the reader of the resources used to conduct the work reported herein.